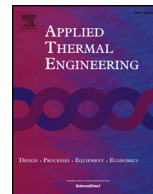




ELSEVIER

Contents lists available at ScienceDirect

## Applied Thermal Engineering

journal homepage: [www.elsevier.com/locate/apthermeng](http://www.elsevier.com/locate/apthermeng)

# A comprehensive thermal assessment of dry cooled supercritical CO<sub>2</sub> power cycles

M. Monjurul Ehsan<sup>a,\*</sup>, Sam Duniam<sup>a</sup>, Jishun Li<sup>b</sup>, Zhiqiang Guan<sup>a</sup>, Hal Gurgenci<sup>a</sup>, Alexander Klimenko<sup>a</sup>

<sup>a</sup> School of Mechanical and Mining Engineering, The University of Queensland, Brisbane, QLD 4072, Australia

<sup>b</sup> School of Mechatronics Engineering, Henan University of Science and Technology, Luoyang, Henan, China

## HIGHLIGHTS

- NDDCT is designed for the recompression and partial cooling sCO<sub>2</sub> cycles.
- Optimum operating conditions are rectified prior to the modelling of NDDCT.
- An iterative method for modelling the finned tube heat exchanger unit is used.
- Impact of ambient temperature is investigated on the cycle performance.
- A comparative study between the recompression and partial cooling cycle.

## ARTICLE INFO

### Keywords:

Supercritical CO<sub>2</sub>  
Concentrated solar  
Cooling system  
Heat exchange  
Recompression  
Partial cooling

## ABSTRACT

In arid areas, dry cooling technology is a preferable alternate of wet cooling mainly owing to the scarcity of abundant water supply. However, the supercritical CO<sub>2</sub> power cycle still offers considerable thermal performance even at higher ambient temperature using dry cooling. The novelty of this work is the exhaustive designing of dry cooler for supercritical CO<sub>2</sub> cycles (recompression and partial cooling) in concentrating solar power application. Prior to the design of tower, a preliminary analysis is conducted in achieving the optimum main compressor inlet temperature (33 °C-recompression and 40 °C-partial cooling) at which the cycle delivers the maximal efficiency. The comparison is performed at same higher and lower pressure and for the partial cooling, the intermediate pressure is optimized. At relatively higher compressor inlet temperatures (above 50 °C), the partial cooling achieves higher efficiency while at lower temperatures (30–49 °C), the recompression shows superior performance. An iterative nodal method is used for the air-cooled finned tube heat exchanger units that takes account of the dramatic variation in thermodynamic properties of CO<sub>2</sub> with the bulk temperature. Kroger's detailed methodology of designing dry cooler is adapted with the implementation of nodal approach for CO<sub>2</sub> property variation. A dry cooling tower with 52.45 m height is essential for the recompression cycle, whereas the partial cooling requires two towers of the height of 35.4 m and 38.7 m. A thermal assessment is carried out on the dry cooler under various cycle fluid inlet temperatures and ambient temperatures. During hot and humid ambient conditions, lower compressor inlet temperatures (up to 53.1 °C) are obtained with the recompression cycle compared to partial cooling (up to 64.5 °C). In extreme climate condition of 50 °C air temperature, the recompression cycle provides superior thermal efficiency (46.5% against 45.5%). For future commercialization of dry cooled sCO<sub>2</sub> power plant, the recompression cycle is preferred due to its superior performance and lower capital cost for cooling tower design and solar field. The work demonstrates the impact of dry cooling tower design strategy in the context of cycle thermal assessment under various working condition.

## 1. Introduction

There has been increased attention lately on concentrating solar

power (CSP) because of its ability to compensate for the intermittency of other renewable sources [1]. CSP today employs subcritical steam Rankine cycles but there is a global drive to replace it with a

\* Corresponding author.

E-mail address: [m.ehsan@uqconnect.edu.au](mailto:m.ehsan@uqconnect.edu.au) (M. Monjurul Ehsan).

supercritical CO<sub>2</sub> (sCO<sub>2</sub>) Brayton cycle to reduce the capital cost [2,3]. The attractive thermodynamic properties of sCO<sub>2</sub> (lower critical temperature and pressure, high isobaric specific heat and density) near the critical condition (31.1 °C and 7.38 MPa) make it an alternative to steam not only in CSP but also in other advanced power generation with the following advantages over the Rankine cycle [4,5].

- (a) The expansion ratio of sCO<sub>2</sub> Brayton cycle is lower compared to the Rankine cycle and the higher temperature of the turbine exhaust offers further heat recovery by the recuperators. The exhaust pressure for the Rankine cycle is below the atmospheric/subcritical pressure and offers no such potential for further heat recovery.
- (b) For turbine inlet temperatures above 560 °C, the cycle efficiency for sCO<sub>2</sub> recompression cycle is greater than superheated/supercritical steam Rankine cycle.
- (c) The heat rejection in sCO<sub>2</sub> Brayton cycle takes place near the critical point. The high fluid density at compressor inlet reduces the compression work.
- (d) The isobaric heat rejection occurs in supercritical condition reducing heat exchanger pinch point restrictions compared to the Rankine cycle where the steam condenses at a constant temperature. Moreover, in the Rankine cycle, the sub-atmospheric condensation pressure poses the risk of air migration into the circuit causing corrosion problems.
- (e) The compact equipment due to high densities and simple plant layout of sCO<sub>2</sub> Brayton cycle reduces the total cost of the CSP.
- (f) In sCO<sub>2</sub> Brayton cycle, the working fluid always retains its gaseous state with the supercritical condition and no phase change occurs, whereas in Rankine cycle, controlling the dryness fraction of the steam exiting the turbine is a challenge.
- (g) Steam turbine isentropic efficiency drops with size and the drop becomes substantial at sizes below 50 MW [6]. Therefore, steam Rankine power plants are not commercially feasible at sizes below 50 MW and this forces a minimum size for the central tower CSP plants.

The first sCO<sub>2</sub> recuperated Brayton cycle was reported by Feher [7] to attain higher thermal efficiency with more compact heat exchangers. Dostal et al. [8] reported a higher cycle efficiency of up to 47% with the proposed sCO<sub>2</sub> recompression Brayton cycle. Ma and Turchi [9] proposed a several sCO<sub>2</sub> closed-loop Brayton cycle layouts for CSP plants. Besarati and Goswami [10] performed comparative studies of different sCO<sub>2</sub> closed-loop Brayton cycles among which the recompression and the partial cooling cycles provided cycle efficiencies exceeding 50%. Garg et al. [11] compared a trans-critical condensing sCO<sub>2</sub> cycle and a trans-critical steam Rankine cycle to observe the impact of volumetric flow rate and entropy generation in CSP systems. Although sCO<sub>2</sub> cycles were mostly proposed for closed-loop Brayton cycle configurations, the authors [11] proposed a transcritical sCO<sub>2</sub> cycle, where the compression process was carried out by a pump instead of a compressor to handle high-density liquid to augment the overall thermal efficiency of the system. Dyreby et al. [12] considered sCO<sub>2</sub> Brayton cycles with recuperation and recompression for the analysis and optimization. The thermal efficiency was significantly influenced by the pressure ratio and compressor inlet condition. A comprehensive review of heat transfer and pressure drop characteristics of sCO<sub>2</sub> in the horizontal tube was presented by Ehsan et al. [13]. Various sCO<sub>2</sub> heat transfer and friction factor correlations were listed in that article. Several studies also reported on the cycle thermal performance and stability with several arrangements of sCO<sub>2</sub> power blocks integrated with CSP systems [14–19].

Li et al. [20] evaluated the component-wise technical feasibilities and design assessment of recompression cycle in a coal-fired power plant. Park et al. [21] et al. also analyzed the reduction of leveled cost of electricity by 7.8–13.6% using sCO<sub>2</sub> recompression cycle over the steam cycle in coal-fired power plants. Villafana and Bueno [22]

performed parametric optimization and thermo-environmental analysis of sCO<sub>2</sub> power cycle coupled with simple recuperated Brayton cycle. Liu et al. [23] assessed the thermodynamic evaluation in terms of heat transfer coefficient and pressure loss of various CO<sub>2</sub> mixture based working fluids in sCO<sub>2</sub> power cycles applicable for dry cooled CSP plants. Luu et al. [24] proposed advanced control strategies of sCO<sub>2</sub> recompression cycle and the dynamic operation under variant solar insolation.

### 1.1. sCO<sub>2</sub> power cycles integrated with dry cooling unit

CSP plants are usually situated in dry areas where freshwater is scarce and dry cooling is the norm. Various studies demonstrated that sCO<sub>2</sub> power cycles perform well even with dry cooling [4,25–28]. Compared to fan-cooled systems, dry cooling using Natural Draft Dry Cooling Towers (NDDCT) offers advantages of reduced parasitic losses and lower operating and maintenance costs. Since heat rejection process in a sCO<sub>2</sub> power cycle takes place near the critical condition, where the physical properties of sCO<sub>2</sub> change with bulk temperature, efficient design of NDDCT is important as it directly affects the cycle performance. Ehsan et al. [29,30] modelled the NDDCT operating with sCO<sub>2</sub> for direct and indirect arrangement of the cooling circuit. Duniam et al. also conducted a study of the direct and indirect arrangement of the dry cooling tower [31]. In direct cooling, the sCO<sub>2</sub> is cooled directly by air; in indirect cooling, a secondary cooling circuit is used where water-cooled by air cools sCO<sub>2</sub>. The lower compressor inlet temperature is achieved with the direct cooling system. A MATLAB code used for designing the cooling system in [29,30] but the NDDCT model was not equipped with the power block. Most of the research articles studying the cycle performance and the compressor inlet condition prescribed by dry cooling with no details of the cooling system. Few studies (Milani et al. [28], Conboy et al. [25], Moiseyev and Sienicki [32], Zeyghami and Khalili [33], and Li et al. [34]) used dry cooling unit by evaluating the cooling duty of the air-cooler.

### 1.2. Research status and scope

Many past studies highlight the potential of super critical CO<sub>2</sub> cycles for power generation with the emphasis on higher thermal efficiencies. Only a few articles deal with the dry cooling option and even then, in a cursory section where the dry cooling equipment is included only as black boxes with prescribed compressor inlet temperature. This is not adequate because our past papers [29,30] found the performance of the sCO<sub>2</sub> cycle being significantly influenced by the cooling system parameters. Moreover, the power cycle performance determines the duty of the cooling system and the cooling system performance in turn influences the power cycle efficiency. For future employment of dry cooled sCO<sub>2</sub> CSP plant, a comprehensive design methodology of NDDCT is required since it is the only viable cooling option in arid areas. The specific climate conditions and the layout/type of sCO<sub>2</sub> power block significantly impact the design of the cooling tower. This research gap is identified and current work will address this by conducting a comprehensive thermal assessment of dry cooler in sCO<sub>2</sub> power cycles for CSP application. The originality of this work is the exhaustive designing of the dry cooling tower based on optimal main compressor inlet temperature for the recompression and partial cooling sCO<sub>2</sub> cycle by applying the nodal approach in the heat exchangers inside the tower. The emphasis will be on the design of NDDCT and the power block. The work presented here is novel in terms of sizing the dry cooling tower (detailed specification of finned tube heat exchanger units and tower construction) working with sCO<sub>2</sub> and its impact on the power cycle thermal performance. The design of the solar field and CSP tower is not considered in the present study. Specifically, the scope of the present article is as follows:

- (a) Two configurations of sCO<sub>2</sub> power cycles (Recompression cycle and

partial cooling cycle) are investigated. Prior to the cooling system modelling, a preliminary analysis with a gas cooler is conducted in Section 4 to obtain an optimal working condition at various compressor inlet temperature, for which the NDDCT is modeled.

- (b) The NDDCT design recognizes the  $s\text{CO}_2$  property variation in the air-cooled heat exchanger, as discussed in Section 5. Since the critical point for  $\text{CO}_2$  is around  $32^\circ\text{C}$ , its physical properties vary wildly while the hot  $s\text{CO}_2$  is cooled by air to near- or below its critical point. An iterative approach is essential in designing the heat exchanger unit.
- (c) The NDDCTs are designed for a 25 MW CSP plant with detailed modeling approach adapted from Kroger's method. The performance of both cycle layouts equipped with NDDCT is conducted in Section 6 under the variant cycle fluid inlet condition inside NDDCT and the air temperature.

The power cycles are optimized on the basis of thermal efficiency. Although the cycle net power generation at lower ambient temperature/compressor inlet temperature increases, this occurs by the expense of higher thermal energy supplied from the CSP components. This consequently increase the capital cost of the solar field with lower design point compressor inlet temperature. Hence, the design point compressor inlet temperature is selected based on the working conditions to attain maximal thermal efficiency.

## 2. Cycle modelling

Two promising configurations of  $s\text{CO}_2$  Brayton cycle are studied in the current analysis. The following assumptions are made during the modelling of the power cycles.

- (a) The heat loss to the surroundings for all components is negligible (except for NDDCT).
- (b) The variations in the kinetic and potential energy of the working fluid are assumed to be insignificant.
- (c) The recuperators are considered as counter-current arrangement and are sectioned into small subsections to predict accurate temperature profiles.
- (d) The thermal energy supplied in the heat source is varied so that the desired cycle highest temperature is achieved.
- (e) The pinch point constriction in the Low-Temperature Recuperator (LTR) is fixed. This parameter determines the split ratio between the recompression (RC) and main compression compressor (MC).
- (f) The fluid streams at the high-pressure outlet of LTR attain the same temperature before the heat exchange in the High-Temperature Recuperator (HTR).

### 2.1. The recompression cycle

The  $s\text{CO}_2$  recompression Brayton cycle eliminates the pinch point phenomenon of the recuperative cycle by employing two recuperators and two compressors. The fraction of mass that flows into the NDDCT is a very important parameter known as a split ratio. This fraction is cooled to the required temperature by NDDCT and then is compressed by the MC compressor. The part that bypasses the NDDCT is compressed to the cycle higher pressure by the RC compressor. The mass split is controlled so that the temperatures of the two fluid streams are equal as they enter the flow mixer before the HTR. For a CSP plant, the heat source in Fig. 1 represents the heat input either directly from the solar field or from thermal storage. In either case, in the present analysis, we assume this heat input to vary so as to maintain a required cycle highest temperature. After expansion, the turbine exhaust transferences its unutilized heat to the high-pressure gas in the recuperators before the flow is split.

### 2.2. The partial cooling cycle

The partial cooling  $s\text{CO}_2$  Brayton cycle adds a second cooler and another compressor to the recompression cycle, shown in Fig. 2. There is no split after the LTR. The entire turbine exhaust is sent to NDDCT-1 and is then compressed to an intermediate pressure in the Pre-Compressor (PC). The flow is split after the PC. One part is cooled by NDDCT-2 and compressed to the turbine inlet pressure by MC. The other part is compressed again in RC. Intercooling part of the stream lowers the total compression work at the expense of extra complexity.

## 3. Model validation

For model validation, results are compared with past studies ([8,35;10]). The cycle efficiency with turbine inlet temperature in recompression and partial cooling cycles is demonstrated in Fig. 3. The various parameters for the validation study are listed in Table 1. Compared to the literature, the model shows good agreement. The slight deviation from the literature is due to the differences in the recuperator representation. In the literature ([8,35;10]), they modelled the recuperators by defining the heat exchanger effectiveness, whereas, in the present work, the temperature difference constraint in the LTR is fixed. The other difference is due to the setting of the intermediate pressure. In the present study, the intermediate pressure is optimized for each condition set. Past studies do not describe how they determine the intermediate pressure. This validated model provides a pathway to model the concentrated solar power system integrated with  $s\text{CO}_2$  power cycles.

## 4. Evaluation of optimum design condition for NDDCT

In the preliminary analysis, the power cycle modelling with standard cooler provided in IPSEpro is conducted to obtain the optimal working condition for which the cycle delivers the highest efficiency. This provides the lowest temperature of each cycle layout, at which the NDDCT will be designed. The design methodology of NDDCT is discussed in Section 7 based on the design parameter evaluated from Section 6. Table 2 provides a complete definition of the boundary conditions for both cycles considered in this study. The selection of air temperature considerably influences the sizing of the tower. Currently,  $20^\circ\text{C}$  chosen as the design point temperature based on the average ambient temperature in Australia. For other specific location, this value should be revised accordingly. However, this work still applies to other ambient conditions.

### 4.1. The recompression $s\text{CO}_2$ cycle

For the recompression power block, the influence of plant lower pressure on the cycle thermal efficiency,  $\eta$  and the split ratio,  $SR$  is studied for a turbine inlet pressure and temperature of 20 MPa and  $650^\circ\text{C}$  respectively. The analysis was repeated for three different main compressor inlet pressures: 8 MPa, 9 MPa, and 10 MPa. The  $SR$  is evaluated based on the boundary conditions imposed on the cycle components [8,10]. The  $SR$  determines the amount of flow bypass to NDDCT and it is optimized in the present work. For each pressure, the efficiency curve peaks near the respective pseudocritical temperature ( $33^\circ\text{C}$  for 8 MPa,  $40^\circ\text{C}$  for 9 MPa and  $45^\circ\text{C}$  for 10 MPa), as shown in Fig. 4(a). The highest  $\eta$  of 51.37% is obtained at  $33^\circ\text{C}$  for 8 MPa case. For higher temperature, the trend of the  $\eta$  curve changes. Therefore, during high ambient temperature period, the higher main compressor inlet temperature,  $MCIT$  is compensated by increasing the cycle lower pressure for the equivalent accomplishment of thermal efficiency.

Similarly, the influence of cycle higher pressure is shown in Fig. 4(b) for a cycle lower pressure of 8 MPa. At main compressor inlet temperatures less than  $40^\circ\text{C}$ , the higher turbine inlet pressures deliver higher thermal efficiencies, but the marginal is reduced at higher

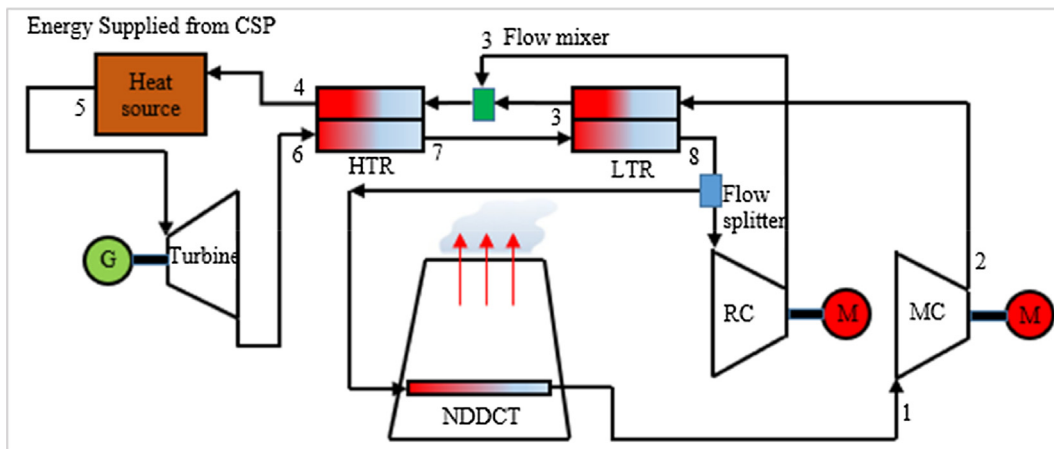


Fig. 1. The sCO<sub>2</sub> recompression cycle integrated with dry cooling.

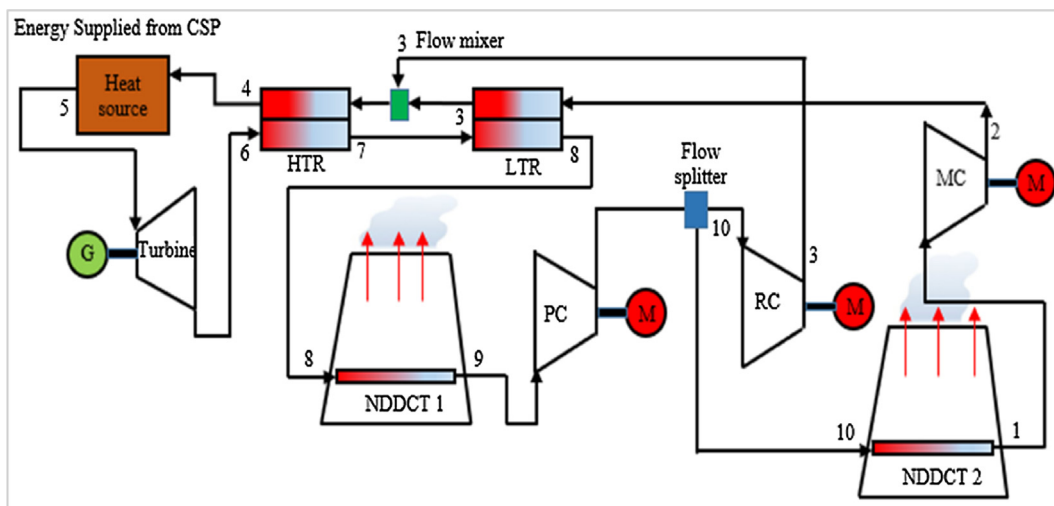


Fig. 2. The sCO<sub>2</sub> partial cooling cycle integrated with NDDCTs.

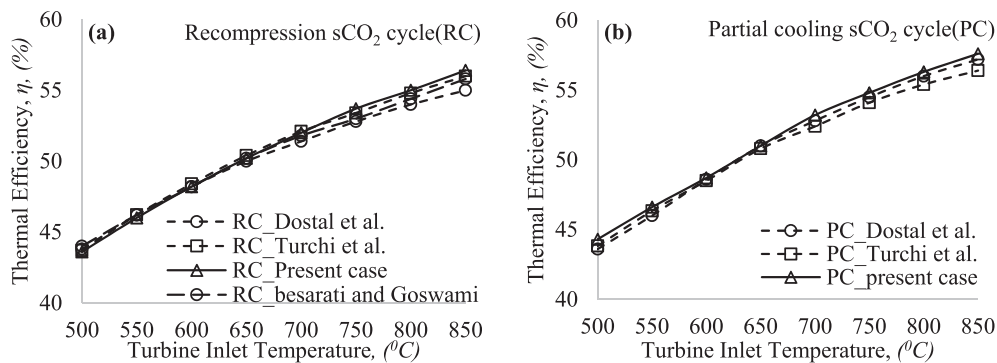


Fig. 3. Model validation for (a) recompression cycle, RC and (b) the partial cooling cycle, PC against literature.

pressures. At higher compressor inlet temperatures, the trend is reversed with lower turbine inlet pressures delivering higher efficiencies although the difference is smaller. Operating the cycle as high as 20 MPa with high-density sCO<sub>2</sub> is challenging as there is little experience with current turbomachinery technologies. Therefore, for the purpose of this analysis, we have compared the relative merits of recompression and partial cooling cycles with 20 MPa and 8 MPa chosen as the cycle higher and lower pressure respectively

The variation of main compressor outlet temperature (MCOT),  $W_{net}$  and heat rejection at various CIT is shown in Fig. 5(a) for the recompression cycle operating at a turbine inlet pressure of 20 MPa and

exhaust pressure of 8 MPa. In Fig. 5(b), the change of SR and  $\eta$  are plotted against the main MCOT. The efficiency is maximum about 33 °C for the compressor inlet pressure of 8 MPa. The SR also varies at different MCIT in order to preserve the temperature constraint set at LTR. Fig. 6 reveals the required mass flow rate for 25 MW recompression Brayton cycle. Since there is no constraint on the heat supply, both the net work and the heat rejection increase with increasing mass flow rate.

#### 4.2. The partial cooling cycle

For the analysis of the partial cooling cycle, the cycle higher and

**Table 1**  
Cycle parameters for model validation against various literature.

Parameter	Value	Remarks
Efficiency of turbine	93%	90% used for recompression cycle
Efficiency of compressor	89%	
Recuperators effectiveness	95%	Pinch point temperature 5 °C is used
Main Compressor inlet temperature	32 °C	
Turbine inlet temperature	500–850 °C	
Maximum cycle pressure	25 MPa	
Cycle lower pressure	7.4 MPa	
Cycle intermediate pressure	–	Optimized for the partial cooling cycle

**Table 2**  
Operating parameters for 25 MW sCO<sub>2</sub> cycle modelling.

Parameter	Recompression cycle	Partial cooling cycle
Efficiency of turbine	0.93	0.93
Efficiency of compressor	0.89	0.89
Mechanical losses	0%	0%
Cycle highest temperature	650 °C	650 °C
Main Compressor inlet temperature	30–70 °C	30–70 °C
Ambient air condition	20 °C, 1 m/s, 0.1 MPa	20 °C, 1 m/s, 0.1 MPa
Maximum cycle pressure	20 MPa	20 MPa
Cycle lower pressure	8 MPa	8 MPa
Cycle intermediate pressure	–	9–14 MPa
Pinch point temperature constraint	5 °C	5 °C

lower pressure are kept at 20 MPa and 8 MPa respectively. Fig. 7(a) plots how the cycle work output comes down with the MCIT at different intermediate pressures (main compressor inlet pressure). This figure shows how sensitive the partial cooling cycle is to the cooling tower exit temperature. Increasing the cycle intermediate pressure increases the  $W_{net}$ . The cycle shows better robustness for the higher intermediate pressure of 11 MPa and 12 MPa cases. However, to maintain operation under optimized conditions, if the cycle intermediate pressure is increased, then one also needs to increase the  $M_s$  and  $SR$  as demonstrated in Fig. 7(b). The influence of intermediate pressure on the  $\eta$  is revealed in Fig. 7(c) for various MCIT conditions. For each operating pressure, the  $\eta$  is maximum close to its respective pseudocritical temperature. The cycle intermediate pressure of 11 MPa is found to be the optimum intermediate pressure for the partial cooling cycle. For higher compressor inlet temperature, the 11 MPa case shows higher efficiency for MCIT = 45 °C and MCIT = 50 °C cases. Increasing the intermediate pressure also increases the power consumption by the compressors, as shown in Fig. 7(d). The total compression work rises from 6.73 MW to 8.63 MW when the intermediate pressure increases from 9 MPa to

14 MPa. For 11 MPa intermediate pressure, the increase of pre-compressor, the recompression compressor and the main compressor outlet temperature with various CIT are shown in Fig. 8(a). The cycle  $SR$  varies with the change of MCIT in order to maintain the constraint set in the recuperator. Certainly, increasing the MCIT, reduces the  $W_{net}$ ,  $\eta$  and heat rejection, as shown in Fig. 8(b).

### 4.3. Cycle comparison

The two cycles are compared against each other for the same operating higher and lower pressure of 20 MPa and 8 MPa. For the partial cooling cycle, the intermediate pressure needs to be increased in order to obtain equivalent or higher  $\eta$ . If the intermediate pressure is increased, the partial cooling cycle can deliver higher  $\eta$  and better robustness at higher MCIT as shown in Fig. 9(a). At lower intermediate pressures (9 MPa and 10 MPa), the partial cooling cycle efficiency  $\eta$  is always lower than that of the recompression cycle. Another figure of comparison is the pinch point temperature difference because the value of the pinch point difference influences the cost and choice of the heat exchanger. As depicted in Fig. 9(b), the recompression cycle is more sensitive to pinch point temperature difference and its work output drops much quicker at higher pinch temperature differences.

### 5. Methodology of NDDCT modelling

Knowing the optimal working condition obtained from the previous section, the tower is now integrated into the sCO<sub>2</sub> power cycle. Horizontally placed air-cooled heat exchanger bundles are employed in this study. The tubes in the bundles are arranged in staggered configurations. Transversal rounded fins are being attached to the tubes to augment the air-side heat transfer surface area, as demonstrated in Fig. 10. The draft force is created because of the temperature variation between the hot inside air and outside ambient air. The higher the temperature variance and height of the tower, the larger the draft. The draft is balanced by the total resistance to flow at the operating point.

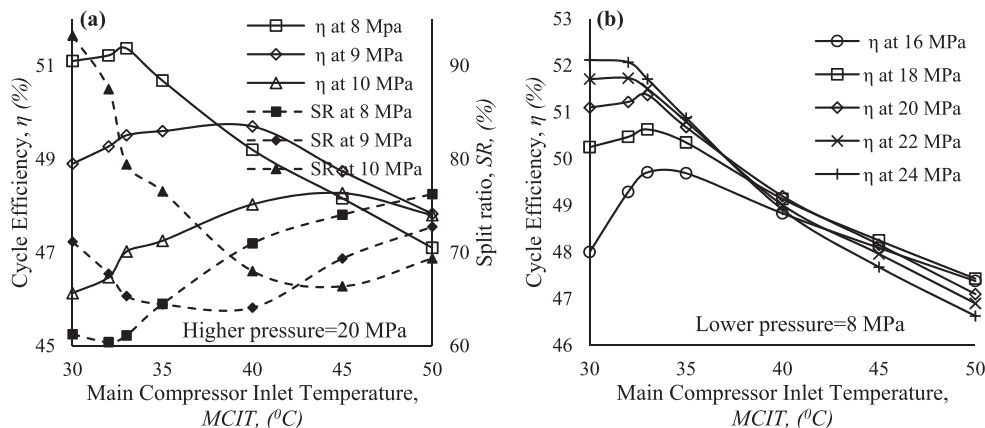


**Fig. 4.** Variation of thermal efficiency at different (a) cycle lower pressure and (b) cycle higher pressure with compressor inlet temperature.

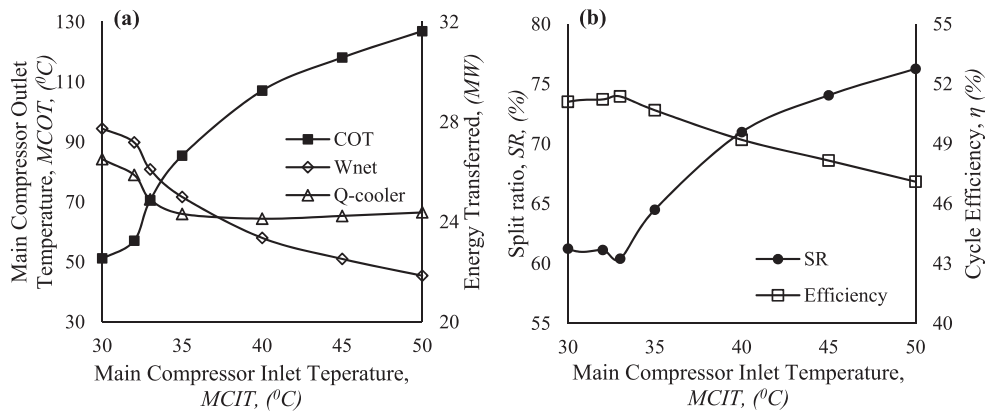


Fig. 5. Influence of compressor inlet temperature on (a)  $COT$ ,  $W_{net}$  and heat rejection and (b) thermal efficiency and split ratio.

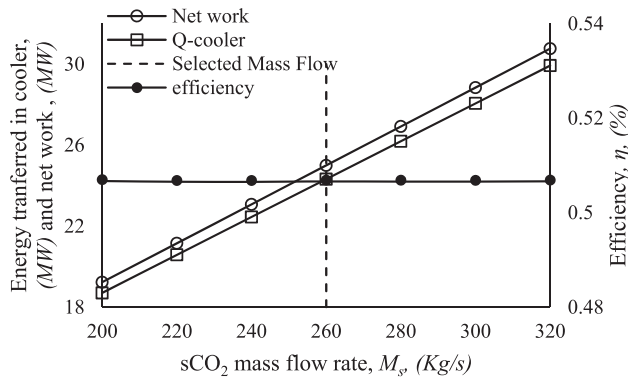


Fig. 6. Selection of mass flow rate for the recompression cycle.

The energy equations for airside and cycle fluid side are outlined as follows.

$$Q_a = M_a C_{pa34} (T_{a4} - T_{a3}) = Q_s = M_s C_s (T_{si} - T_{so}) \quad (1)$$

$$Q_{hx} = \frac{UAF_T [(T_{si} - T_{a4}) - (T_{so} - T_{a3})]}{\ln \left[ \frac{(T_{si} - T_{a4})}{(T_{so} - T_{a3})} \right]} \quad (2)$$

Here,  $Q_a$ ,  $Q_s$  and  $Q_{hx}$  are the heat transfer in airside,  $sCO_2$  side and heat exchanger respectively.  $M_a$  and  $M_s$  are the mass flow rates and  $C_{pa34}$  mean air side specific heat evaluated at the mean of  $T_{a4}$  and  $T_{a3}$ .  $T_{si}$  and  $T_{so}$  are the  $sCO_2$  inlet and outlet temperatures. Different subscripts on temperature,  $T$ , height,  $H$ , area,  $A$  diameter,  $d$ , density  $\rho$ , and pressure  $P$  represent various location inside the NDDCT.

The draft equation is expressed as,

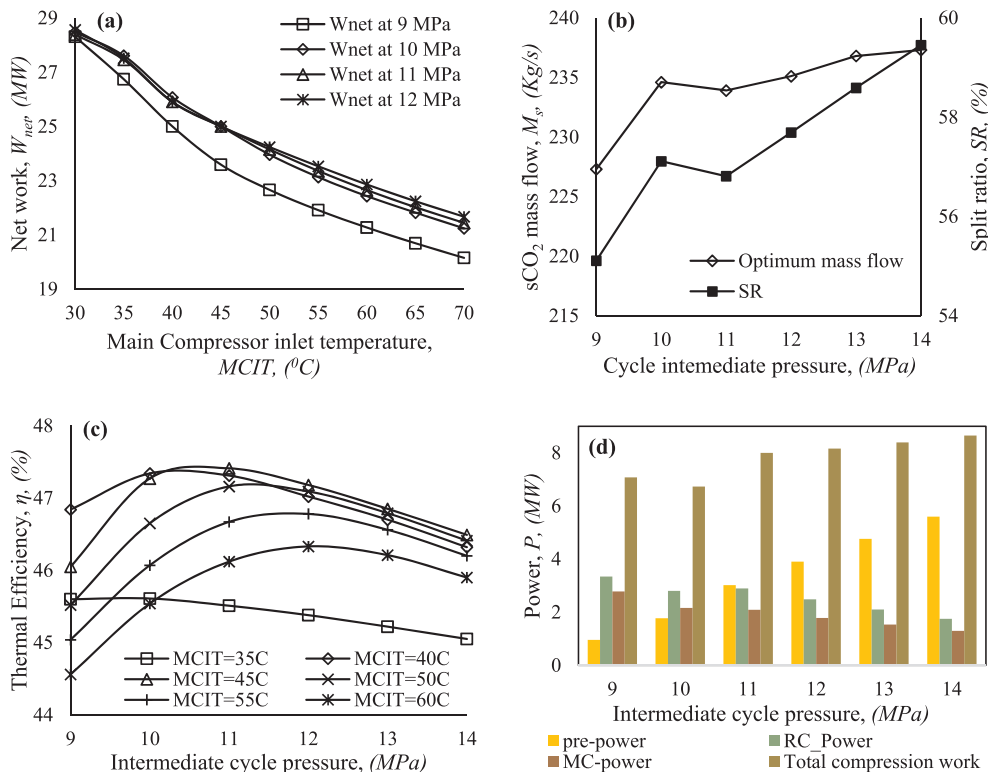


Fig. 7. Influence of intermediate pressure on (a)  $W_{net}$ , (b) mass flow and split ratio, (c) cycle efficiency, and (d) power of compressors.

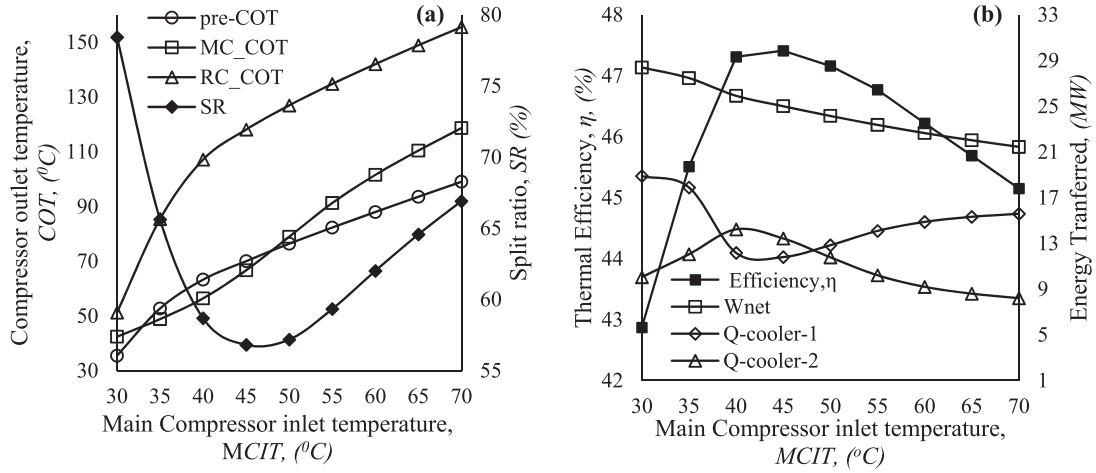


Fig. 8. Influence of CIT on the (a) pre, recompression, and main compressor outlet temperature and the split ratio, and (b) thermal efficiency,  $W_{net}$ , and heat rejection. The intermediate pressure = 11 MPa.

$$\begin{aligned}
 P_{a1} &= \left[ P_{a5} + \frac{\left(\frac{m_a}{A_s}\right)^2}{2\rho_{a5}} \right] \\
 &= (K_{ts} + K_{ct} + K_{hes} + K_{ctc} + K_{he} + K_{cte}) \frac{\left(\frac{m_a}{A_{fr}}\right)^2}{2\rho_{a34}} + P_{a1} \\
 &\left[ 1 - \left\{ 1 - 0.00975 \frac{(H_3 + H_4)}{2T_{a1}} \right\}^{3.5} \right] + P_{a4} \left[ 1 - \left\{ \right. \right. \\
 &\left. \left. 1 - 0.00975 \left( H_5 - \frac{H_3}{2} - \frac{H_4}{2} \right) T_{a4} \right\}^{3.5} \right] \quad (3)
 \end{aligned}$$

Table 3 lists all the equations used to evaluate the loss coefficients. The draft equation takes account of these losses. Temperature, density, and pressure at various sections of the tower are given below. Table 4 lists the important constitutional relationships, Table 5 shows the evaluation of parameters for correction factor and Table 6 displays the details of the heat exchanger bundles. The temperature gradient  $dT_a/dz$  takes account of the ambient temperature drop from the ground level and this occurs in the region of the surface boundary layer. This allows correct interpretation of cooling tower dataset. Another parameter, air porosity  $\sigma_a$  depends on the fin specification and tube outside diameter which significantly impacts the fin effectiveness. According to our heat exchanger specification, the  $\sigma_a$  is 0.44 which provides the fin effectiveness within the design limit.

$$T_{a6} = T_{a1} - 0.00975H_6 \quad (4)$$

$$T_{a5} = T_{a4} - 0.00975(H_5 - H_4) \quad (5)$$

$$T_{a3} = T_{a1} - 0.00975H_3 \quad (6)$$

$$\begin{aligned}
 P_{a4} &= P_{a1} \left[ 1 - 0.00975 \frac{(H_3 + H_4)}{2T_{a1}} \right]^{3.5} - (K_{ts} + K_{ct} + K_{hes} + K_{ctc} + K_{he} + K_{cte} \\
 &\left. \left( \frac{m_a}{A_{fr}} \right)^2 \right) \frac{1}{2\rho_{a34}} \quad (7)
 \end{aligned}$$

$$P_{a6} = P_{a1} \left( 1 - 0.00975 \frac{H_5}{T_{a1}} \right)^{3.5} \quad (8)$$

$$P_{a5} = P_{a6} + \Delta P_{a56} = P_{a6} + K_{l0} \frac{\left(\frac{m_a}{A_s}\right)^2}{2\rho_{a5}} \quad (9)$$

$$\rho_{a6} = \frac{P_{a6}}{RT_{a6}} = \frac{P_{a6}}{R[T_{a1} - 0.00975H_6]} \quad (10)$$

$$\rho_{a5} = \frac{P_{a5}}{RT_{a5}} = \frac{P_{a5}}{R[T_{a4} - 0.00975(H_5 - H_4)]} \quad (11)$$

$$\rho_{a4} = \frac{P_{a1}}{RT_{a4}} \quad (12)$$

$$\rho_{a3} = \frac{P_{a1}}{RT_{a3}} = \frac{P_{a1}}{R[T_{a1} - 0.00975H_3]} \quad (13)$$

$$\frac{1}{\rho_{a34}} = 0.5 \left( \frac{1}{\rho_{a3}} + \frac{1}{\rho_{a4}} \right) = 0.5R(T_{a3} + T_{a4})/P_{a1} \quad (14)$$

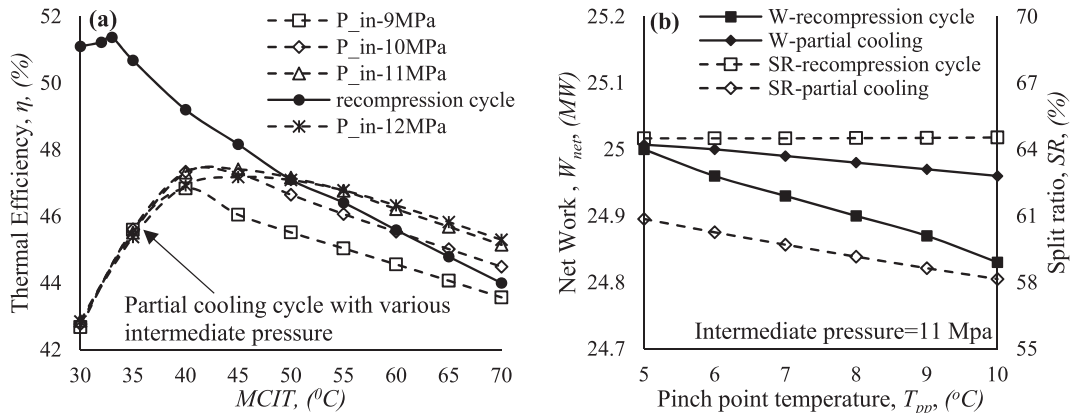


Fig. 9. Cycle performance comparison with respect to (a) MCIT and (b) pinch point temperature constraint.

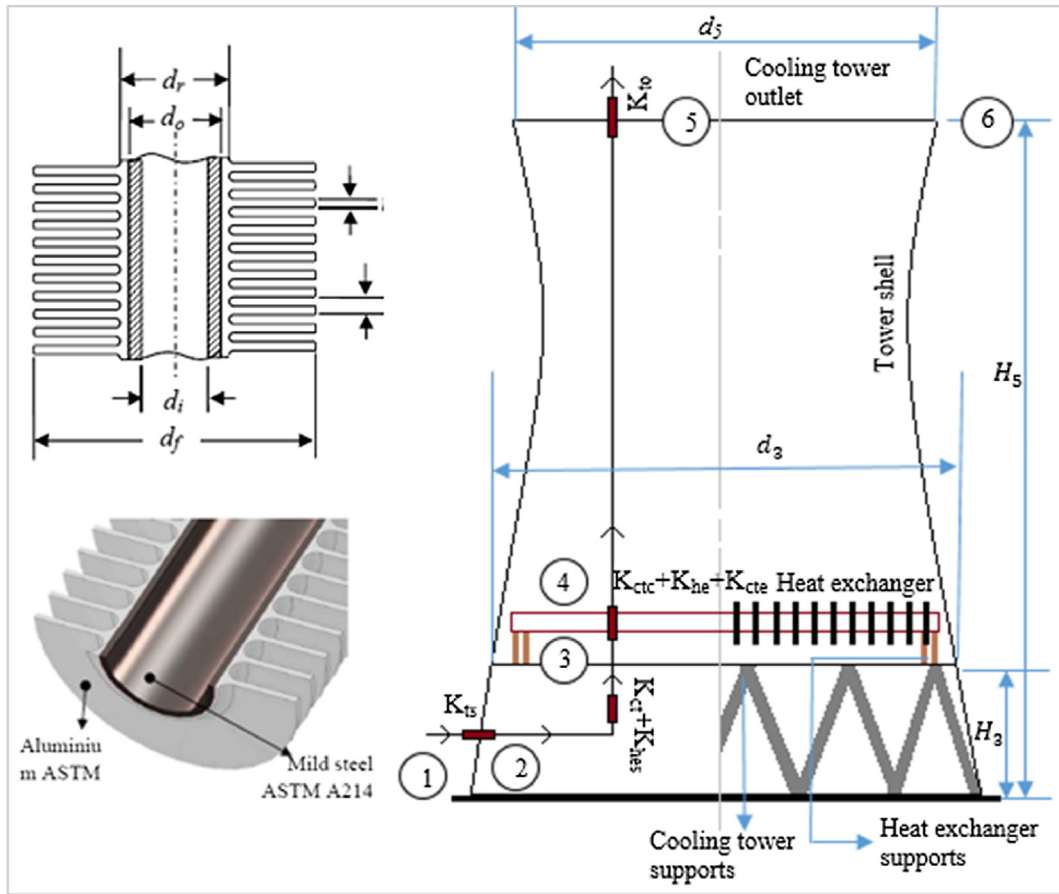


Fig. 10. The nomenclature used for modelling of the finned tube heat exchanger and various losses encountered by the airstream at different parts of NDDCT.

Yoon et al. [38] correlation is used for the determination of the heat transfer coefficient of sCO<sub>2</sub>. The value of coefficients a, b, and c are reported in [38].

$$Nu_s = a Re_s^b Pr_s^c \left( \frac{\rho_{pc}}{\rho_s} \right)^n \quad (15)$$

The UA value is expressed by

$$UA = \left[ \frac{1}{(h_s A_s)} + \frac{1}{2\pi k_b n_b n_{tb} L} \ln \frac{d_o}{d_i} + \frac{1}{2\pi k_f n_b n_{tb} L} \ln \frac{d_f}{d_o} + \frac{1}{(h_a e_f A_{aT})} \right]^{-1} \quad (16)$$

The temperature correction factor,  $F_T$  is calculated by

$$F_T = 1 - \sum_{i=1}^4 \sum_{k=1}^4 a_{i,k} (1 - \varphi_3)^k \sin \left[ 2i \arctan \left( \frac{\varphi_1}{\varphi_2} \right) \right] \quad (17)$$

$$\varphi_1 = \frac{(T_{s1} - T_{s0})}{(T_{s1} - T_{a3})}$$

Table 3  
Flow resistance equations for NDDCT modelling.

Loss Coefficient	Equation
Support loss efficient [36], $K_{ts}$	$K_{ts} = \frac{C_{Dis} L_{ts} d_{ts} n_{ts} A_{fr}^2}{(\pi d_3 H_3)^3} \left( \frac{\rho_{a34}}{\rho_{a1}} \right)$ Here, $C_{Dis}$ , $L_{ts}$ , $d_{ts}$ , and $n_{ts}$ represents drag coefficient, length, diameter, and the number of tower supports respectively
Contraction loss efficient, [36], $K_{ctc}$	$K_{ctc} = \left( 1 - \frac{2}{\sigma_c} + \frac{1}{\sigma_c^2} \right) \left( \frac{\rho_{a34}}{\rho_{a1}} \right) \left( \frac{A_{fr}}{A_{e3}} \right)^2$ Here, $\sigma_c$ is the contraction ratio depends on geometry.
Expansion loss efficient, [36], $K_{cte}$	$K_{cte} = \left( 1 - \frac{A_{e3}}{A_3} \right)^2 \left( \frac{\rho_{a34}}{\rho_{a1}} \right) \left( \frac{A_{fr}}{A_{e3}} \right)^2$
Cooling tower inlet loss coefficient, $K_{ct}$	Preetz and Kroger [37] correlation, $K_{ct} = \left[ -18.7 + 8.095 \left( \frac{d_3}{H_3} \right) - 1.084 \left( \frac{d_3}{H_3} \right)^2 + 0.0575 \left( \frac{d_3}{H_3} \right)^3 \right] \times K_{he}^{[0.165 - 0.035 \left( \frac{d_3}{H_3} \right)]}$
Cooling tower outlet loss coefficient [36], $K_{io}$	$K_{io} = -0.28 Fr_D^{-1} + 0.04 Fr_D^{-1.5} Fr_D = \left( \frac{Ma}{A_5} \right)^2 / [ \rho_{a5} (\rho_{a6} - \rho_{a5}) g d_5 ]$ $Fr_D$ is the Froude number
Heat exchanger loss coefficient, [36], $K_{he}$	Characteristic Reynolds number, $Ry = \frac{Ma}{\mu_{a34} A_{frT}}$ $K_{he} = 31383.9475 Ry^{-0.332458} + \frac{2}{\sigma_a^2} \left( \frac{\rho_{a3} - \rho_{a4}}{\rho_{a3} + \rho_{a4}} \right)$

**Table 4**  
Geometric construction details of a finned tube heat exchanger.

Parameter	Equation	Parameter	Equation
The free flow area of control volume, $A_{cvc}$	$A_{cvc} = (P_t - d_r)(P_f - t_f)$	Total air side surface area, $A_{aT}$	$A_{aT} = (A_f + A_r)n_b$
The frontal area of the control volume, $A_{cvfr}$	$A_{cvfr} = P_t P_f$	Equivalent hydraulic diameter, $d_{ca}$	$d_{ca} = \frac{4A_{cvc}P_t}{A_{cva}}$
The overall fin surface area for a control volume, $A_{cva}$	$A_{cva} = 2 \left[ P_t P_l - \frac{\pi}{4} d_o^2 \right] + \pi d_r (P_f - t_f)$	The air porosity, $\sigma_a$	$\sigma_a = \frac{A_{cvc}}{A_{cvfr}}$
The overall effective air-side fin surface area, $A_f$	$A_f = n_r n_{tr} \frac{L_t}{P_f} \left[ \pi \left\{ \frac{2}{4} (d_f^2 - d_r^2) + d_f t_{fr} \right\} \right]$	Fin efficiency, $\eta_f$	$\eta_f = \frac{\tanh\left(\frac{bd_r \varphi}{2}\right)}{\left(\frac{bd_r \varphi}{2}\right)} b = \left[ \frac{2ha}{(k_f t_f)} \right]^{0.5} \varphi = \left( \frac{d_f}{d_r} - 1 \right) \left[ 1 + 0.35 \ln \left( \frac{d_f}{d_r} \right) \right]$
The exposed root area, $A_r$	$A_r = \pi n_r n_{tr} L_t d_r (P_f - t_f) / P_f$	Fin effectiveness, $e_f$	$e_f = 1 - \frac{A_f}{A_a} (1 - \eta_f)$

**Table 5**  
Evaluation of  $a_{i,k}$  for correction factor.

$a_{i,k}$	i = 1	i = 2	i = 3	i = 4
k = 1	-1.14 × 0.01	-1.39 × 0.01	-7.23 × 0.001	6.10 × 0.001
k = 2	6.15 × 0.1	1.23 × 0.1	5.66 × 0.01	-4.68 × 0.01
k = 3	-1.20	-3.45 × 0.1	-4.37 × 0.01	1.07 × 0.1
k = 4	2.06	3.18 × 0.1	1.11 × 0.01	-7.57 × 0.01

$$\varphi_2 = \frac{(T_{a4} - T_{a3})}{(T_{s1} - T_{a3})}$$

$$\varphi_3 = \frac{(\varphi_1 - \varphi_2)}{\ln \left[ \frac{(\varphi_1 - \varphi_2)}{(1 - \varphi_2)/(1 - \varphi_1)} \right]}$$

The computation of  $a_{i,k}$  is given from the following Table 5. The conventional technique of designing the heat exchanger is not sufficient for sCO<sub>2</sub> cooling. The conventional procedures such as using LMTD or NTUs are based on nominally constant thermodynamic properties. The rapid changes of sCO<sub>2</sub> thermodynamic properties near the critical point make these methods inapplicable. An iterative approach is applied that considers the property changes with the change of temperature. The heat exchangers are discretized as a series of subdivisions and the log mean technique is used in every small subdivision to capture the local bulk fluid properties. This approach allows the prediction of the local fluid properties along the length. It is noted that

**Table 6**  
Fixed geometric parameters for cooling tower modelling.

Parameter	Value	Parameter	Value
<i>Specification of heat exchanger</i>			
Tube material	ASTM A214 mild steel	Fin type	Extruded bimetallic
Fin material	ASTM 6063 aluminium	Heat exchanger arrangement	horizontal
Fin Shape	Circular	Tube arrangement	staggered
Tube thermal conductivity, $k_t$	50 W/mK	Fin thermal conductivity, $k_f$	204 W/mK
Tube outside diameter, $d_o$	25.4 mm	Fin diameter, $d_f$	57.2 mm
Tube inside diameter, $d_i$	21.6 mm	Fin root diameter, $d_r$	27.6 mm
Relative tube surface roughness, $\epsilon/d_i$	$5.24 \times 10^{-4}$	Fin shape	Tapered
Quantity of tube rows, $n_r$	4	Fin tip thickness, $t_{ft}$	0.27 mm
Tubes per bundle, $n_b$	154	Fin thickness (mean), $t_f$	0.49 mm
Transversal tube pitch, $P_t$	58 mm	Fin root thickness, $t_{fr}$	0.7 mm
Longitudinal tube pitch, $P_l$	50.22 mm	Fin Pitch, $P_f$	2.7 mm
Tube length, $L_t$	15 m	Air porosity, $\sigma_a$	0.44
<i>Specification of NDDCT</i>			
Aspect ratio of cooling tower, $H_3/d_3$	1.4	Length of tower support: $l_{ts}$	$(H_3 \times 1.15)$ m
Tower inlet height, $H_3$	$(d_3/6.5)$ m	Support drag coefficient, $C_{Dis}$	2
Tower Diameter ratio, $d_5/d_3$	0.7	Thickness of tower support, $d_{ts}$	0.5 m
Heat exchanger coverage of tower inlet, $A_{frT}/A_3$	0.65	Quantity of tower supports: $n_{ts}$	$d_3/1.38$
<i>Ambient Air Condition</i>			
Air inlet temperature at ground level, $T_{a1}$	20 °C	Temperature gradient: $dT_a/dz$	-0.00975 K/m
Pressure at ground level, $P_{a1}$	99695 N/m <sup>2</sup>	Relative humidity, $W_a$	60%
Wind Speed, $V_a$	1.0 m/s	Universal gas constant, $R$	287.08 J/kgK

detailed modelling of the recuperators and turbo-machineries are not considered in the present work. The fluid in the state in these components is away from the critical point and conventional methods do apply. The modelling of the power cycles integrated with NDDCT model is conducted with the simulation software IPSEpro [39]. The modelling of NDDCT is performed by the model development kit (MDK) provided by IPSEpro. The sCO<sub>2</sub> thermodynamic properties are evaluated by the property software package, REFPROP [40]. Table 7 shows the cycle duty requirements of NDDCT modelling. The two critical parameters for the NDDCT design are the design values of the tower cycle fluid temperature and the environmental temperature. Fig. 11 demonstrates the flowchart followed by the MDK script to model the NDDCT.

The code initiates the calculation with inlet sCO<sub>2</sub> temperature in the tower, ambient temperature with fixed geometric relationships of the tower. The outlet parameters are assumed for heat exchanger segment with a fixed heat exchanger bundles. The equations to calculate the airside properties (thermal properties, partial pressure of water vapor, Reynolds number, humidity ratio, and local heat transfer) are discussed in ref [36]. The heat exchangers are discretized and the sCO<sub>2</sub> local heat transfer coefficients  $h_s$  are calculated separately for each heat exchanger segment. Pressure losses in all locations of the NDDCT are evaluated using the airflow rate for the current iteration. This is repeated until the iterations converge and a design is found that can handle the required load. Knowing the local fluid properties of both sides of the heat exchanger, the code then evaluates the draft equation with all losses taken into consideration. The air mass flow is the solution from the draft

**Table 7**  
Cycle duty requirements for NDDCT modelling.

Parameter	Recompression cycle	Partial cooling cycle
Inlet temperature of NDDCT	75 °C	63 °C
Turbine inlet pressure	20 MPa	20 MPa
Turbine exhaust pressure	8.0 MPa	8.0 MPa
Cycle intermediate pressure	–	11 MPa
Cycle mass flow	248.7 Kg/s	226.2 Kg/s
Air ambient temperature	20 °C	20 °C
Plant thermal output	25 MW	25 MW

equation which allows calculating the heat dissipation in the tower. The code alters the initial estimates (air outlet temperature and heat

exchanger bundles) if the desired MCIT/NDDCT exit temperature is not achieved.

Table 8 lists what the script calculated as sizes of the tower and the heat exchangers that will deliver the duty specified in the previous table. For the recompression cycle, the NDDCT of 52.4 m height is necessary whereas for partial cooling cycle two cooling towers are required with heights of 38.7 m and 35.4 m. In Section 6, the thermal performance of the two-cycle layouts equipped with NDDCT is compared under various sCO<sub>2</sub> inlet temperature inside NDDCT and ambient temperature.

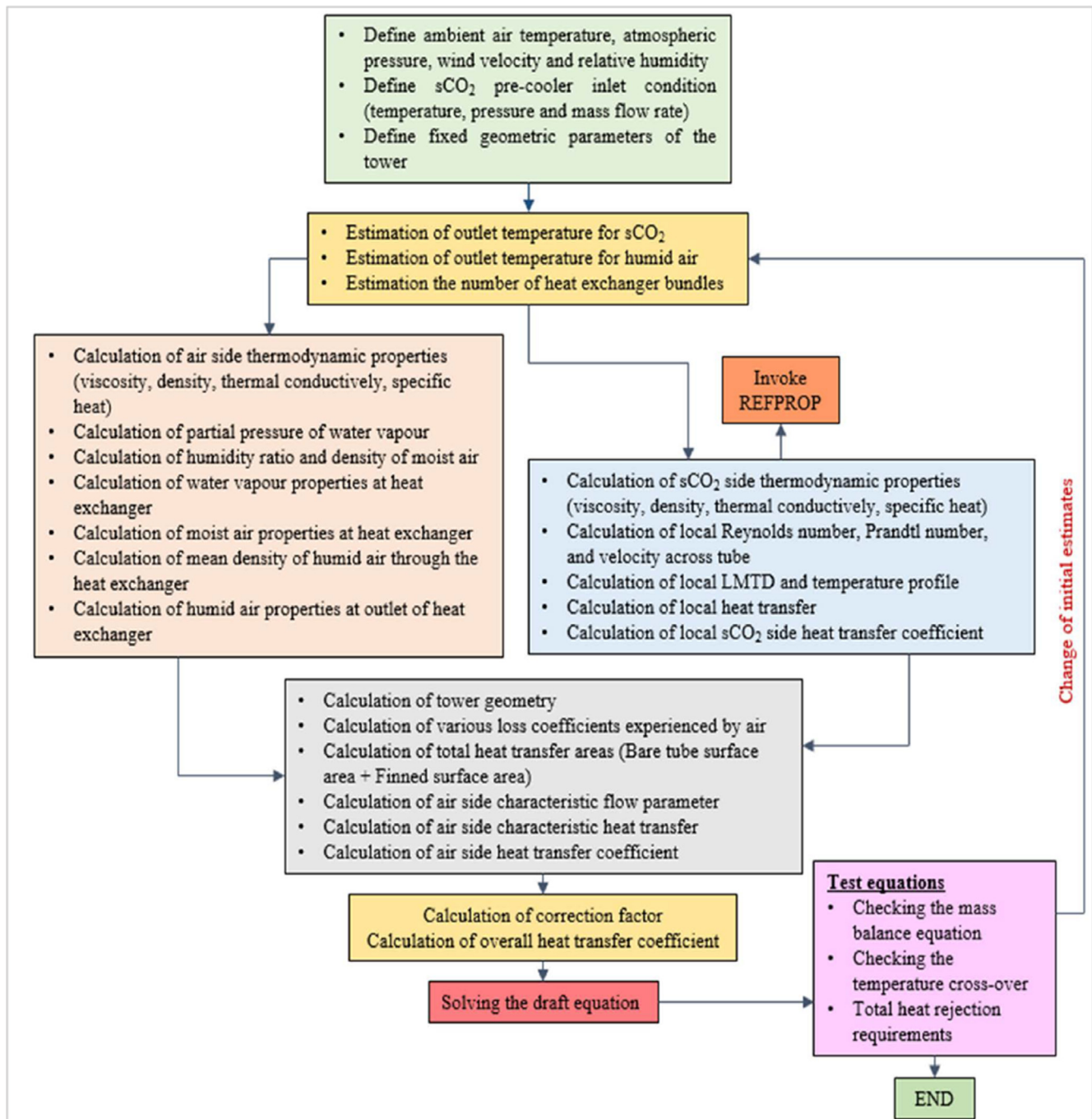


Fig. 11. NDDCT modelling procedure by MDK.

**Table 8**  
NDDCT size for specific duty requirements.

Parameter	Recompression cycle	Partial cooling cycle	
		NDDCT-1	NDDCT-2
Outlet height of the tower, $H_5$	52.45 m	38.7 m	35.4 m
Outlet diameter, $d_5$	26.22 m	19.4 m	17.7 m
Inlet diameter, $d_3$	37.46 m	27.66 m	25.25 m
Quantity of finned tube bundles, $n_b$	22	12	10
Quantity of NDDCT supports: $n_{ts}$	27	20	18
Dimension of NDDCT support: $l_{ts}$	6.65 m	4.92 m	4.5 m
Overall air side surface area	5,27,127 m <sup>2</sup>	2,87,524 m <sup>2</sup>	2,39,603 m <sup>2</sup>
Overall tube side surface area	3924 m <sup>2</sup>	2140 m <sup>2</sup>	1,783 m <sup>2</sup>
Cycle fluid outlet temperature	33.1 °C	40.1 °C	39.9 °C

## 6. Thermal assessment of power cycles equipped with NDDCT

### 6.1. NDDCT inlet temperature variation

The impact of varying the inlet sCO<sub>2</sub> temperature in NDDCT on the thermal performance of NDDCT is shown in Fig. 12(a) and (b) for the recompression and partial cooling cycle respectively. By increasing the inlet temperature, heat dissipated by the tower rises for both cycles. The variation of heat transferred by the recuperators is also shown in these figures. For both cycles,  $Q_{HTR}$  decreases and  $Q_{LTR}$  increases with the increase of sCO<sub>2</sub> inlet temperature. The  $\eta$  sharply decreases since more heat energy are required to be added to the heat source for the acquisition of higher inlet temperature in NDDCT, as revealed in Fig. 13(a). For partial cooling cycle, the heat input to the cycle is higher compared to the recompression cycle due to lower heat source inlet temperature of the high-pressure stream. The turbine inlet temperature is always kept at 650 °C to perform the inlet temperature variation. Fig. 13(b) demonstrates the PC and MC inlet temperature and mass flow rate at a various sCO<sub>2</sub> inlet temperature of NDDCT. For the recompression cycle, the compressor inlet temperature remains almost constant and lower in comparison with the partial cooling cycle. The mass flow rate for the recompression cycle is higher than the partial cooling cycle.

### 6.2. Air temperature variation

The thermal performance of NDDCT is expressively impacted by the air temperature. Increasing the air temperature from 15 °C to 50 °C,

reduces the heat transferred by the HTR and for LTR, the heat transfer almost remains constant, as shown in Fig. 14(a). Heat dissipated by the tower and heat addition in the heat source heat exchanger both declines with air temperature. Certainly, the  $CIT$  for the recompression cycle increases from 31.1 °C to 53.1 °C and the  $M_a$  in tower drops from 1181 Kg/s to 990 Kg/s, shown in Fig. 14(b). Similarly, for the partial cooling cycle, the influence of air temperature is shown in Fig. 15(a) and (b). Likewise, the recompression cycle, all the parameters  $Q_{HTR}$ ,  $Q_{LTR}$ , and  $Q_{heat\ source}$  decrease with the increase in air temperature. For ambient temperature up to 25 °C, the  $M_a$  value for NDDCT-2 is higher compared to NDDCT-1. From 25 °C air temperature onwards, the trend of the air mass flow reverses. However, for both towers,  $M_a$  decreases with the rise air temperature. For NDDCT-1, the heat rejection merely increases (13.5–15.1 MW) whereas, for NDDCT-2, the heat rejection decreases from 15.7 MW to 10.1 MW. This variation is due to the change of  $SR$  which consequently changes the inlet condition of NDDCT's at various ambient temperature.

The iterative section method adapted in the heat exchanger inside the NDDCT allows the examination of sCO<sub>2</sub> local  $h_s$ , local bulk temperature,  $T_s$ , tube side local Reynolds number,  $Re$  as demonstrated in Fig. 16(a) and (b) for the recompression cycle. The profiles are shown for three cases of ambient air (20 °C, 25 °C, and 30 °C). Since sCO<sub>2</sub> is cooled, the  $T_s$  decreases along the heat exchanger length. For an ambient temperature of 20 °C, when the  $T_s$  approaches near to its pseudocritical temperature, a sharp rise of  $h_s$  is observed at 80% tube length. For the other two cases, the  $h_s$  keeps increasing till the end of the tube and the pseudocritical temperature is not reached. At the inlet of the heat exchanger, the  $T_s$  is higher which yields lower viscosity and density for which the  $Re$  is higher at the inlet of the tube. As the  $T_s$  gradually decreases, the  $Re$  value also decreases due to higher fluid density. Moreover, at higher air temperature, the  $Re$  value also increases due to higher  $T_s$ . In Fig. 17(a) and (b) the variation  $T_s$  and  $h_s$  is shown for the partial cooling cycle for both NDDCTs. Likewise, the recompression cycle, similar  $T_s$  profile is observed. Since the NDDCT-1 operates at a lower pressure of 7.96 MPa, the  $T_s$  profile of sCO<sub>2</sub> never reaches to its pseudocritical temperature ( $T_{pc} = 34.6$  °C for 7.96 MPa). Hence the  $h_s$  keeps increasing with the decrease of  $T_s$  till the end of the pipe for NDDCT-1. However, the NDDCT-2 operates at cycle intermediate pressure of 11 MPa and for all three cases of air temperature (20 °C, 25 °C, and 30 °C), the  $T_s$  approaches to its pseudocritical temperature ( $T_{pc} = 49.8$  °C for 11 MPa). Therefore, a sharp rise of  $h_s$  is observed as the  $T_s$  approaches pseudocritical temperature for NDDCT-2 of the partial cooling cycle.

It is well known that the  $MCIT$  considerably impacts the cycle performance. Hence, in Fig. 18(a), the increase of  $MCIT$  with air temperature is shown for the recompression and partial cooling cycle. For the partial cooling cycle, PC compressor inlet temperature and MC

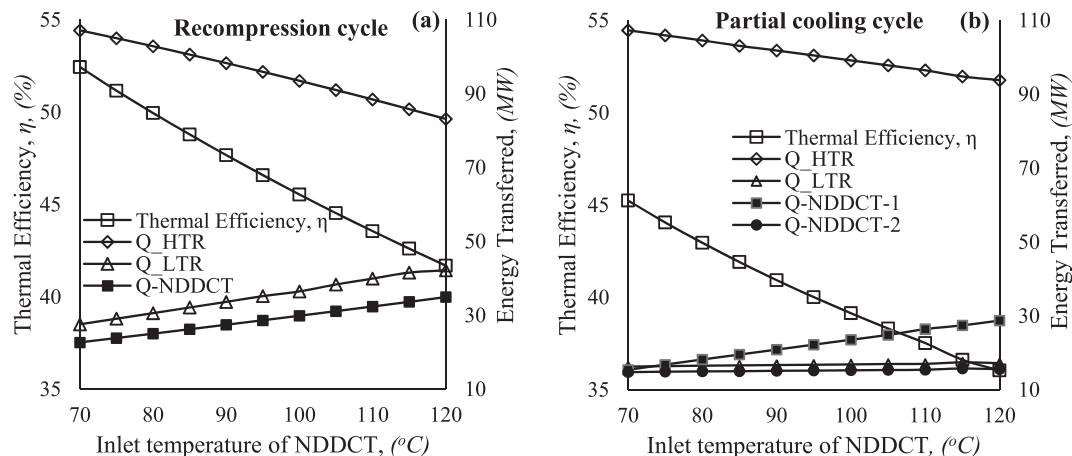


**Fig. 12.** Impact of sCO<sub>2</sub> temperature on (a) the recompression cycle and (b) the partial cooling cycle.

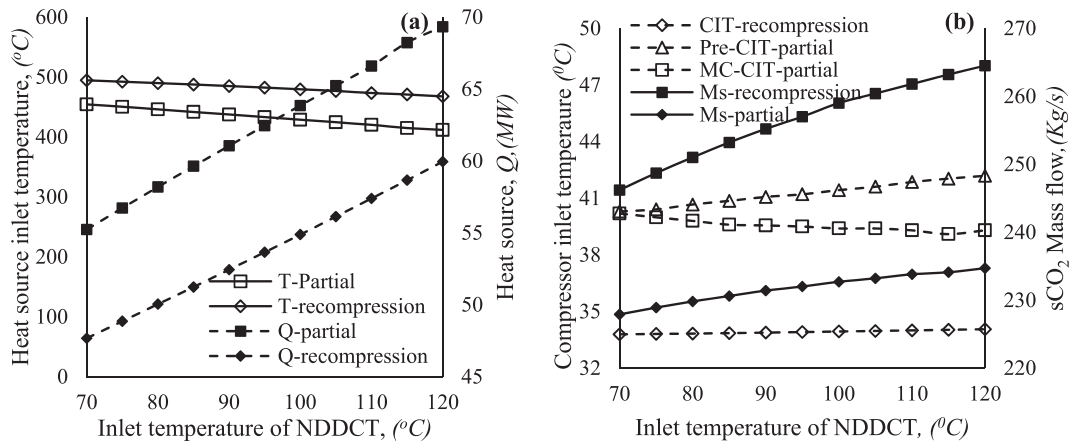


Fig. 13. Variation of  $sCO_2$  temperature on (a) the heat source heat exchanger and (b) the compressor and cycle mass flow rate.

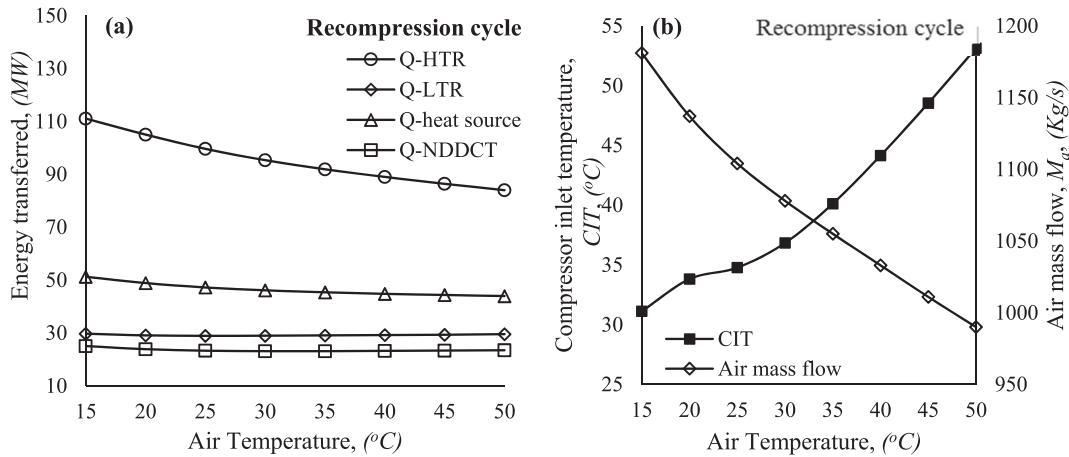


Fig. 14. Air temperature variation on (a) heat transfer rate, (b) CIT, and airflow in NDDCT for the recompression cycle.

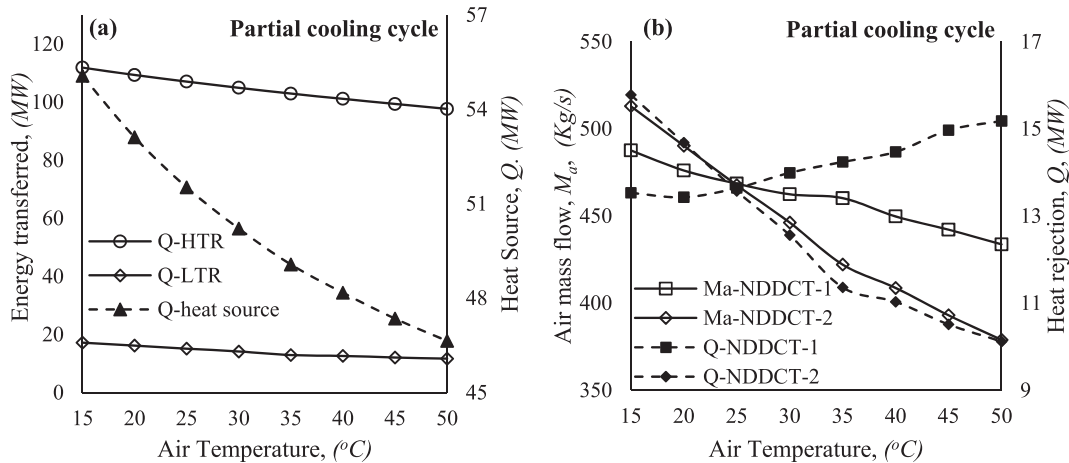


Fig. 15. Air temperature variation on (a) heat transfer rate, (b) heat rejection, and airflow in NDDCTs for the partial cooling cycle.

compressor inlet temperature are not equal. The accomplishment of ideal intercooling is not observed. The lower  $MCIT$  in the recompression cycle yields higher  $\eta$  during high ambient temperature period, as shown in Fig. 18(b). The change in  $SR$  for both cycles at various air temperature is also shown. For the recompression cycle, the highest  $\eta$  is achieved at 20 °C air temperature which gives the compressor inlet temperature of 33.1 °C. As the ambient temperature increases,  $\eta$  decreases from 51.17% to 46.5%.

In the preliminary analysis of the cycle, it is shown that for the same

operating condition, the partial cooling cycle provides the higher  $\eta$  when the main compressor inlet temperature is more than 50 °C compared to the recompression cycle. However, when the cycle is integrated with a detailed model of NDDCT, even at an air temperature of 50 °C, the recompression cycle always retains its lower compressor inlet temperature range in comparison with the partial cooling cycle. For the recompression cycle, CIT increases up to 53.13 °C which is sufficiently lower than partial cooling cycle. Hence, higher cycle  $\eta$  is obtained with recompression cycle. If theoretically, the  $MCIT$  further increases for

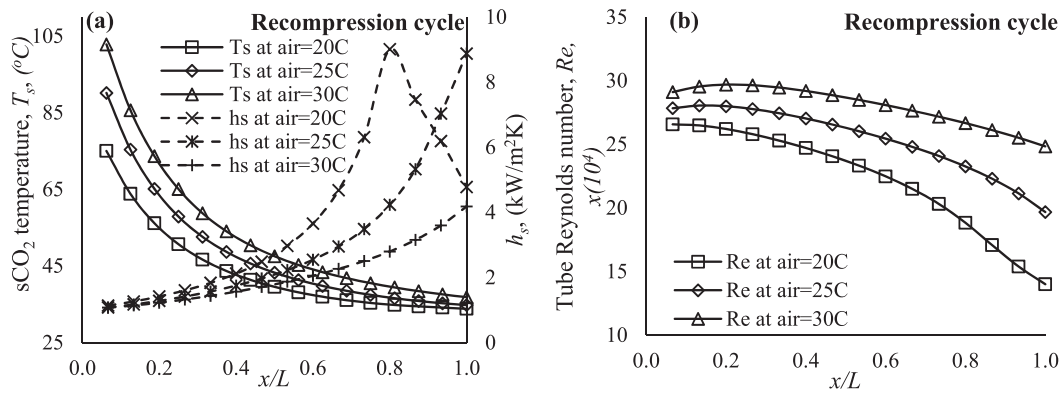


Fig. 16. Profiles for (a) cycle fluid temperature and lengthwise heat transfer profiles and (b) local Reynolds number in the tubes of the heat exchanger.

both cycles, the partial cooling cycle would provide higher efficiency and better robustness in comparison with the recompression cycle. However, in a more realistic situation when the cycle is coupled with NDDCT, at various air temperature, the recompression cycle shows better thermal performance. However, a higher  $W_{net}$  can be obtained from the partial cooling cycle during high ambient temperature period, as shown in Fig. 19. The total compression work,  $W_c$  for the recompression cycle increases from 7.7 MW to 13.5 MW, whereas for partial cooling cycle it is from 6.1 MW to 10.5 MW. The improvement of  $W_{net}$  for the partial cooling cycle is 1.7–4.2% in comparison with the recompression cycle. But again, the heat input to the cycle is higher for the partial cooling cycle in comparison with the recompression cycle.

7. Conclusion

In the present work, a dry cooling system is modelled for both recompression and partial cooling  $sCO_2$  cycles applicable for CSP plant. In arid of CSP application, a comprehensive analysis of constructing dry cooling tower is necessary especially when the working fluid is  $sCO_2$ . This involves additional precaution in constructing the finned tube heat exchanger units within the NDDCT. The choice of design-point air temperature based on a specific location is important in evaluating the cooling duty and sizing the tower. The choice of power block significantly impacts on the overall size of the cooling tower. Initially, a preliminary analysis is carried out with the standard model of the gas cooler to explore an optimum operating condition for which the NDDCT is designed. Summary of the major findings is described below.

- The influence of various cycle pressures is investigated. For the partial cooling cycle, intermediate pressure significantly affects the cycle performance, hence it is optimized. Both cycles are compared for the same operating higher and lower pressure. For the recompression cycle, the lower compressor inlet temperature is not

always desired for attaining higher  $\eta$ , especially with  $sCO_2$ . In order to achieve higher thermal efficiency, the cycle lower pressure should be close to the critical condition of  $CO_2$ . The  $\eta$  is maximum near to the pseudocritical temperature. For the partial cooling cycle, increasing the cycle intermediate pressure yields higher  $W_{net}$  but there is an optimum operating pressure at which both cycle the  $\eta$  and  $W_{net}$  are maximum.

- The impact of the compressor inlet temperature on the  $\eta$ , turbine work, compressor work, and heat transfer by the recuperators and cooler is investigated. The lower compressor inlet temperature is obtained for the recompression cycle, whereas at relatively higher values, the partial cooling cycle provides better performance based on the  $W_{net}$  generated. Based on the outcome, an optimum operating condition is prescribed for both cycles for which the cooling tower is designed.
- The section approach is adapted in the heat exchanger modelling inside the NDDCT. This allows the examination of bulk temperature change of  $sCO_2$  and the corresponding lengthwise heat transfer profile within the tube. The recompression cycle necessitates a tower height of 52.45 m whereas, for the partial cooling cycle, two NDDCTs are required with a tower height of 38.7 m 35.4 m, respectively.
- The impact of the  $sCO_2$  temperature inside NDDCT on the thermal performance is performed. The higher inlet temperature inside NDDCT reduces the  $\eta$  for both cycles due to an increase of heat addition to the heat source heat exchanger. During the high ambient temperature period, the lower compressor inlet temperature is achieved with the recompression cycle compared to the partial cooling cycle. Although, the recompression cycle shows higher  $\eta$ , the  $W_{net}$  by the cycle is higher for the partial cooling cycle.

For large scale power generation, recompression cycle is preferred over the partial cooling or other complicated layouts due to its superior

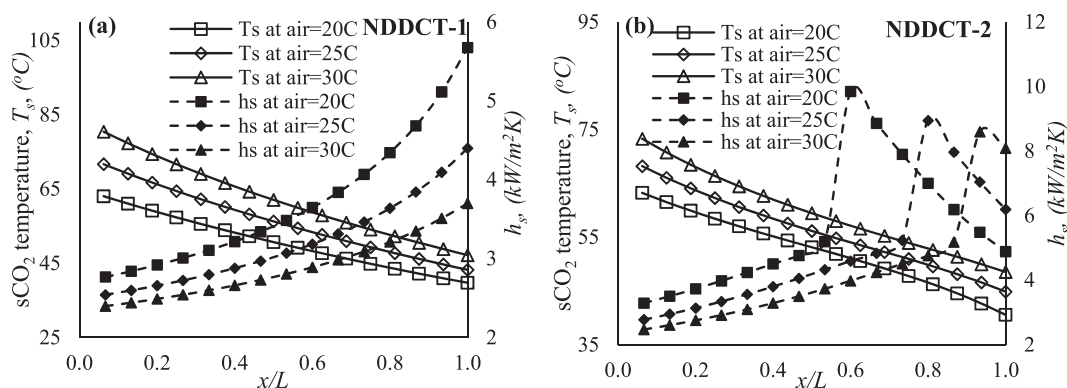


Fig. 17. Variation of the  $T_s$  and  $h_s$  in (a) NDDCT-1 and (b) NDDCT-2 of the partial cooling cycle.

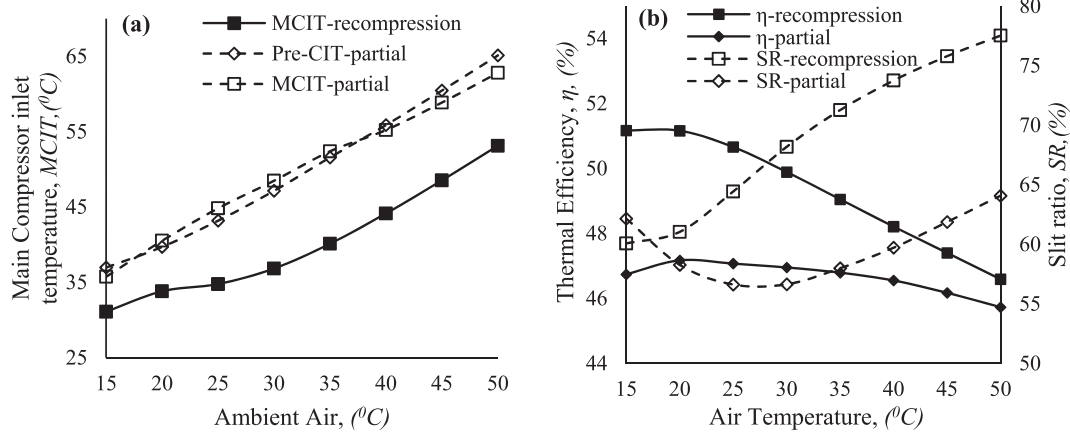


Fig. 18. Cycle performance comparison with respect to (a) MCIT and (b) thermal efficiency and split ratio.

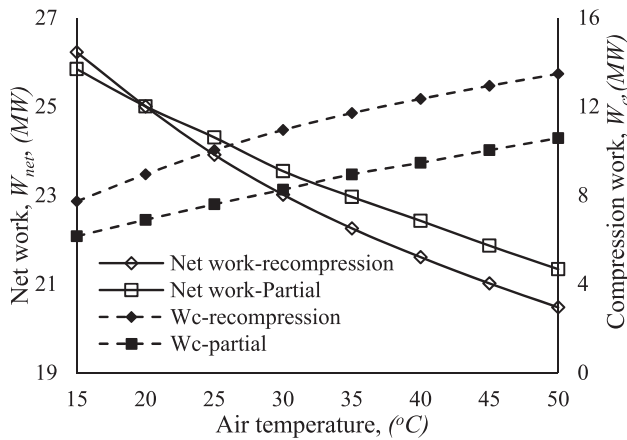


Fig. 19. Comparison of  $W_{net}$  and total compression work for two cycles.

performance in terms of less complexity in the layout and lower capital cost in tower design and solar field. Although the partial cooling generates higher net power compared to recompression, this comes at the expense of higher thermal energy supplied to the cycle which consequently increases the capital cost in sizing the heliostat field and central receiver.

**Declaration of Competing Interest**

The authors declared that there is no conflict of interest.

**Acknowledgment**

Thanks to the University of Queensland (UQ) for Research Training Program award. The project is funded by the Australian Renewable Energy Agency (ARENA) under the supports of Australian Solar Thermal Research Institute (ASTRI).

**Appendix A. Supplementary material**

Supplementary data to this article can be found online at <https://doi.org/10.1016/j.applthermaleng.2019.114645>.

**References**

[1] A.W. Dowling, T. Zheng, V.M. Zavala, Economic assessment of concentrated solar power technologies: a review, *Renew. Sustain. Energy Rev.* 72 (2017) 1019–1032.  
 [2] S. Kim, Y. Cho, M.S. Kim, M. Kim, Characteristics and optimization of supercritical CO2 recompression power cycle and the influence of pinch point temperature difference of recuperators, *Energy* 147 (2018) 1216–1226.

[3] S. Son, J.I. Lee, Application of adjoint sensitivity analysis method to supercritical CO2 power cycle optimization, *Energy* 147 (2018) 1153–1164.  
 [4] J.D. Osorio, R. Hovsapien, J.C. Ordenez, Dynamic analysis of concentrated solar supercritical CO2-based power generation closed-loop cycle, *Appl. Therm. Eng.* 93 (2016) 920–934.  
 [5] K. Wang, M.-J. Li, J.-Q. Guo, P. Li, Z.-B. Liu, A systematic comparison of different S-CO2 Brayton cycle layouts based on multi-objective optimization for applications in solar power tower plants, *Appl. Energy* 212 (2018) 109–121.  
 [6] N.R.E. Laboratory, Assessment of parabolic trough and power tower solar technology cost and performance forecasts (no. 34440), Diane Publishing, 2003.  
 [7] E.G. Feher, The supercritical thermodynamic power cycle, *Energy Convers.* 8 (2) (1968) 85–90.  
 [8] V. Dostal, M.J. Driscoll, P. Hejzlar, N.E. Todreas, A supercritical CO2 gas turbine power cycle for next-generation nuclear reactors, *Proc. ICONE 10* (2002) 2002.  
 [9] Z. Ma, C.S. Turchi, Advanced Supercritical Carbon Dioxide Power Cycle Configurations for Use in Concentrating Solar Power Systems: Preprint, National Renewable Energy Laboratory (NREL), Golden, CO, 2011.  
 [10] S.M. Besarati, D.Y. Goswami, Analysis of advanced supercritical carbon dioxide power cycles with a bottoming cycle for concentrating solar power applications, *J. Sol. Energy Eng.* 136 (1) (2014) 010904.  
 [11] P. Garg, K. Srinivasan, P. Dutta, P. Kumar, Comparison of CO2 and steam in trans-critical Rankine cycles for concentrated solar power, *Energy Proc.* 49 (2014) 1138–1146.  
 [12] J. Dyreby, S. Klein, G. Nellis, D. Reindl, Design considerations for supercritical carbon dioxide Brayton cycles with recompression, *J. Eng. Gas Turbines Power* 136 (10) (2014) 101701.  
 [13] M.M. Ehsan, Z. Guan, A. Klimenko, A comprehensive review on heat transfer and pressure drop characteristics and correlations with supercritical CO2 under heating and cooling applications, *Renew. Sustain. Energy Rev.* 92 (2018) 658–675.  
 [14] M. Binotti, M. Astolfi, S. Campanari, G. Manzolini, P. Silva, Preliminary assessment of sCO2 cycles for power generation in CSP solar tower plants, *Appl. Energy* 204 (2017) 1007–1017.  
 [15] K. Wang, Y.-L. He, H.-H. Zhu, Integration between supercritical CO2 Brayton cycles and molten salt solar power towers: A review and a comprehensive comparison of different cycle layouts, *Appl. Energy* 195 (2017) 819–836.  
 [16] K. Wang, Y.-L. He, Thermodynamic analysis and optimization of a molten salt solar power tower integrated with a recompression supercritical CO2 Brayton cycle based on integrated modeling, *Energy Convers. Manage.* 135 (2017) 336–350.  
 [17] H.-H. Zhu, K. Wang, Y.-L. He, Thermodynamic analysis and comparison for different direct-heated supercritical CO2 Brayton cycles integrated into a solar thermal power tower system, *Energy* 140 (2017) 144–157.  
 [18] M.M. Ehsan, Z. Guan, H. Gurgenci, A.Y. Klimenko, Irreversibility and exergy analysis of a recompression supercritical CO2 cycle coupled with dry cooling system, in: *ASTFE Digital Library*, Begel House Inc., 2019.  
 [19] M.M. Ehsan, S. Duniam, Z. Guan, H. Gurgenci, A. Klimenko, Seasonal variation on the performance of the dry cooled supercritical CO2 recompression cycle, *Energy Convers. Manage.* 197 (2019) 111865.  
 [20] H. Li, et al., Preliminary design assessment of supercritical CO2 cycle for commercial scale coal-fired power plants, *Appl. Therm. Eng.* 158 (2019) 113785.  
 [21] S. Park, J. Kim, M. Yoon, D. Rhim, C. Yeom, Thermodynamic and economic investigation of coal-fired power plant combined with various supercritical CO2 Brayton power cycle, *Appl. Therm. Eng.* 130 (2018) 611–623.  
 [22] E.D.S. Villafana, J.P.V.M. Bueno, Thermoeconomic and environmental analysis and optimization of the supercritical CO2 cycle integration in a simple cycle power plant, *Appl. Therm. Eng.* 152 (2019) 1–12.  
 [23] X. Liu, Z. Xu, Y. Xie, H. Yang, CO2-based mixture working fluids used for the dry-cooling supercritical Brayton cycle: Thermodynamic evaluation, *Appl. Therm. Eng.* 162 (2019) 114226.  
 [24] M.T. Luu, D. Milani, R. McNaughton, A. Abbas, Advanced control strategies for dynamic operation of a solar-assisted recompression supercritical CO2 Brayton power cycle, *Appl. Therm. Eng.* 136 (2018) 682–700.  
 [25] T. Conboy, M. Carlson, G. Rochau, Dry-cooled supercritical CO2 power for

- advanced nuclear reactors, *J. Eng. Gas Turbines Power* 137 (1) (2015) 012901.
- [26] R.V. Padilla, Y.C.S. Too, R. Benito, W. Stein, Exergetic analysis of supercritical CO<sub>2</sub> Brayton cycles integrated with solar central receivers, *Appl. Energy* 148 (2015) 348–365.
- [27] M.T. Luu, D. Milani, R. McNaughton, A. Abbas, Advanced control strategies for dynamic operation of a solar-assisted recompression supercritical CO<sub>2</sub> Brayton power cycle, *Appl. Therm. Eng.* (2018).
- [28] D. Milani, M.T. Luu, R. McNaughton, A. Abbas, Optimizing an advanced hybrid of solar-assisted supercritical CO<sub>2</sub> Brayton cycle: A vital transition for low-carbon power generation industry, *Energy Convers. Manage.* 148 (2017) 1317–1331.
- [29] M.M. Ehsan, Z. Guan, A. Klimenko, X. Wang, Design and comparison of direct and indirect cooling system for 25 MW solar power plant operated with supercritical CO<sub>2</sub> cycle, *Energy Convers. Manage.* 168 (2018) 611–628.
- [30] M.M. Ehsan, X. Wang, Z. Guan, A. Klimenko, Design and performance study of dry cooling system for 25 MW solar power plant operated with supercritical CO<sub>2</sub> cycle, *Int. J. Therm. Sci.* 132 (2018) 398–410.
- [31] S. Duniyam, I. Jahn, K. Hooman, Y. Lu, A. Veeraragavan, Comparison of direct and indirect natural draft dry cooling tower cooling of the sCO<sub>2</sub> Brayton cycle for concentrated solar power plants, *Appl. Therm. Eng.* 130 (2018) 1070–1080.
- [32] A. Moiseyev, J.J. Sienicki, Investigation of a dry air cooling option for an S-CO<sub>2</sub> cycle, in: *Supercritical CO<sub>2</sub> Power Symposium*, Pittsburgh (PA), 2014.
- [33] M. Zeyghami, F. Khalili, Performance improvement of dry cooled advanced concentrating solar power plants using daytime radiative cooling, *Energy Convers. Manage.* 106 (2015) 10–20.
- [34] L. Li, Y. Ge, X. Luo, S.A. Tassou, Experimental investigation on power generation with low grade waste heat and CO<sub>2</sub> transcritical power cycle, *Energy Proc.* 123 (2017) 297–304.
- [35] C.S. Turchi, Z. Ma, T.W. Neises, M.J. Wagner, Thermodynamic study of advanced supercritical carbon dioxide power cycles for concentrating solar power systems, *J. Sol. Energy Eng.* 135 (4) (2013) 041007.
- [36] D.G. Kröger, *Air-Cooled Heat Exchangers and Cooling Towers*, PennWell Books, 2004.
- [37] A. Du Preez, D. Kröger, The influence of buoyant plume on the performance of a natural draft cooling tower, in: *9th IAHR Cooling Tower and Spraying Pond Symposium*, Brussels, 1994.
- [38] S.H. Yoon, J.H. Kim, Y.W. Hwang, M.S. Kim, K. Min, Y. Kim, Heat transfer and pressure drop characteristics during the in-tube cooling process of carbon dioxide in the supercritical region, *Int. J. Refrig* 26 (8) (2003) 857–864.
- [39] S. IPSEpro, *Process Simulation Environment (PSE)*, Simtech, Austria, 2003.
- [40] E.W. Lemmon, M.L. Huber, M.O. McLinden, *NIST reference fluid thermodynamic and transport properties-REFPROP*, ed: version, 2002.